

# SATGround : A Spatially-Aware Approach for Visual Grounding in Remote Sensing

Aysim Toker\*, Andreea-Maria Oncescu\*, Roy Miles\*, Ismail Elezi\*, Jiankang Deng†  
Huawei London Research Center\*, Imperial College London†

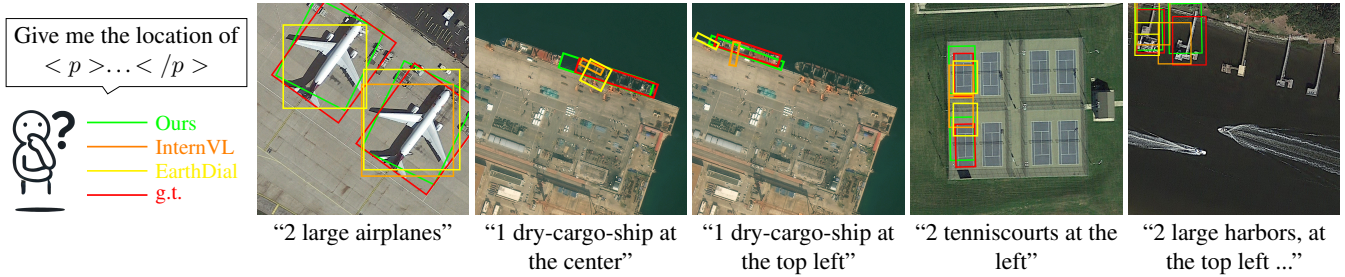


Figure 1. We propose a novel spatially-aware grounding mechanism for vision-language models (VLMs) in remote sensing. Our approach (green) integrates structured spatial information, leading to significantly improved localization capabilities compared to methods that treat bounding boxes as text. The qualitative examples shown here highlight our model’s superior alignment with the ground truth (red) on diverse user prompts, outperforming strong baselines like InternVL [12], CVPR’24 (orange), and EarthDial [51], CVPR’25 (yellow).

## Abstract

*Vision-language models (VLMs) are emerging as powerful generalist tools for remote sensing, capable of integrating information across diverse tasks and enabling flexible, instruction-based interactions via a chat interface. In this work, we enhance VLM-based visual grounding in satellite imagery by proposing a novel structured localization mechanism. Our approach involves finetuning a pretrained VLM on a diverse set of instruction-following tasks, while interfacing a dedicated grounding module through specialized control tokens for localization. This method facilitates joint reasoning over both language and spatial information, significantly enhancing the model’s ability to precisely localize objects in complex satellite scenes. We evaluate our framework on several remote sensing benchmarks, consistently improving the state-of-the-art, including a 24.8% relative improvement over previous methods on visual grounding. Our results highlight the benefits of integrating structured spatial reasoning into VLMs, paving the way for more reliable real-world satellite data analysis.*

## 1. Introduction

The rapid proliferation of Earth observation technologies in recent years has provided unprecedented access to high-resolution satellite imagery, enabling advanced monitoring

and analysis of the Earth’s surface. Extracting actionable insights from this vast data depends on scalable machine learning approaches. Open data initiatives like Landsat [60] and Copernicus [4] have facilitated the curation of specialized datasets for a wide range of applications, including disaster response, food security, and urban growth analysis. These applications require models capable of performing complex tasks, such as object recognition, temporal change detection, and interpreting scene compositionality.

Traditional machine learning approaches tackle these challenges by defining discriminative models for specific tasks such as scene classification or semantic segmentation. More recently, vision-language models (VLMs) have opened up promising new applications for multi-modal satellite data. The advantage of such generalist models lies in large-scale pretraining on image-text pairs and fine-tuning on instructional prompts. Hence, they can leverage prior knowledge about real-world scenes and reason about their content in a dialogue-based format, allowing them to respond to complex user queries. This conversational paradigm, where users issue queries and AI assistants generate responses, enables the joint learning of linguistic and visual semantics. A key question is how we can ensure natural interaction with these models while obtaining precise and accurate information about a given satellite scene.

One common approach is visual grounding for detection, which reinforces the link between textual descrip-

tions of objects and their corresponding visual representation. Following the pioneering approach GeoChat [26], a number of recent works aim to leverage visual grounding for remote sensing tasks through bounding box detection [39, 40, 51, 68]. A common strategy in these approaches is embedding bounding box locations into the prompt by converting them into text form, which may also require assigning special tokens for each possible numeric value. This is straightforward and convenient for interfacing off-the-shelf vision-language models, but it also has significant limitations due to the lack of geometric structure associated with such numerical tokens [48–50]. Without an explicit spatial metric, the model does not have a notion of proximity, decreasing its robustness to small perturbations and out-of-distribution generalization. We show that this can inhibit the localization performance in practice, indicating a demand for more specialized grounding approaches.

In this work, we introduce *SATGround*, a novel grounding technique for vision-language models that integrates multi-modal learning with a specialized localization mechanism for remote sensing data. We adapt existing instruction-following datasets by introducing special tokens which act as anchors for bounding box prediction and localization. Rather than converting bounding boxes into a text representation, our LLM decoder operates simultaneously in language space and bounding box space. This dual approach effectively combines visual and textual semantics while facilitating communication between these two modalities.

*SATGround* is a generalist framework that can be adapted to different remote sensing applications, making it both scalable and highly flexible. Our structured visual grounding technique bridges the gap between language and spatial reasoning, thus improving the localization robustness and consistency across diverse satellite imagery datasets compared to existing grounding approaches. In summary, our **contributions** are the following:

- We **propose** *SATGround*, a novel, spatially-aware localization technique of visual grounding for Earth observation data.
- We **finetune** an existing generalist vision-language model for both language and detection objectives, interfacing these two modalities via special control tokens and a custom localization module.
- We **advance** the state-of-the-art on several remote sensing benchmarks [13, 21, 26, 36, 51], achieving a significant relative improvement of 24.8% in visual grounding performance compared to existing methods.

## 2. Related work

**Vision-language models.** Over the last few years, multi-modal learning for vision tasks has become an extensively studied topic, with various approaches and applications. We provide an overview of techniques most relevant to our

work here and refer to a recent survey [71] for a more comprehensive review of the broader field.

Early multi-modal approaches [25, 37, 45, 62, 64, 67] revolve around a common paradigm where, given large-scale text-image pairs [8, 47], the model aims to integrate features into a joint embedding space with techniques such as contrastive learning. Once the embeddings are learned, this shared space is then leveraged for zero-shot learning across a variety of tasks, such as classification [45, 67], retrieval [17, 32, 43, 55], object detection [3, 32]. Later, numerous extensions were proposed that apply such models to open-vocabulary detection [16, 18, 20, 38], segmentation [56, 57, 61], or 3D open-world learning [72, 78]. Most of these methods focus on pretraining base models and thus require additional finetuning for discriminative tasks.

More recently, models like LLaVA [34] and GPT-4 [2, 76] have introduced assistants capable of processing multi-modal inputs, as well as generating task-specific outputs. LLaVA [34] provides a general framework that combines language instructions and visual embeddings into a single sequence, enabling the use of a pretrained LLM [15, 19, 41, 54, 58] as a decoder. In this work, we adopt a similar strategy, leveraging a pretrained LLM as a decoder to ground a vision-language model for Earth observation tasks.

**Grounding vision-language models.** The goal of visual grounding for localization is to improve the ability of models to identify the location of objects based on text-based queries. Training a VLM typically consists of two stages: a pretraining stage and a visual instruction tuning stage. Several works have proposed to integrate grounding into this second stage by embedding location information into a text representation [11, 42, 59, 63]. This has led to many refined instruction tuning datasets [11, 29, 42, 69] with a focus on referring and grounding tasks. However, a common limitation of all models trained in this way is that they lack any explicit geometric modeling and are contingent on the model’s ability to interpret text-based location information. Prior work has shown [48–50] that language models often struggle with numerical inference tasks and spatial understanding due to challenges arising from default tokenization, positional encoding schemes, and limitations in multi-step reasoning.

A number of works [28, 35, 70, 75] attempted to address this problem by proposing more specialized grounding modules. Unfortunately, these techniques are often highly engineered and specific to common object-centric data [32]. In contrast, we propose a simple new grounding technique for remote sensing data – interfacing a generalist VLM via specialized task tokens and leveraging its rich visual semantic features to predict bounding box coordinates.



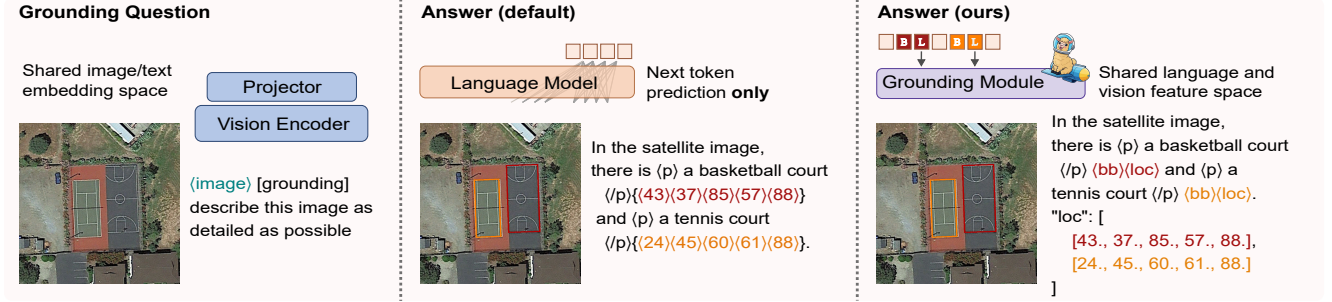


Figure 2. **Structured visual grounding.** For a given user query (left), we visualize the conventional text-based visual grounding approach (middle), compared to our structured explicit grounding format (right). For illustration purposes, we show the ground-truth bounding box location values (red and orange) in both cases. Instead of returning bounding box coordinates as text, we model a dedicated localization mechanism interfaced by special control tokens  $\langle bb \rangle$  and  $\langle loc \rangle$ , see Sec. 3.2 for more details.

**Vision-language models for satellite imagery.** Applying existing VLMs to Earth observation tasks presents a unique set of challenges, as the large domain gap between satellite and natural images often limits their performance on remote sensing data. For an overview of recent works aimed at adapting general multi-modal methods for satellite tasks, we refer to the recent survey by Li et al. [31]. Such approaches leverage task-specific datasets to enhance performance in zero-shot classification [30, 44], image captioning [79], and visual question answering [6, 9, 65]. However, these models are typically limited to specific tasks and lack the ability to engage in instruction-following dialogues.

The pioneering work RSGPT [23] introduces the RSI-Cap dataset to finetune multi-modal models for instruction-following capabilities on remote sensing data, with applications such as image captioning and visual question answering (VQA). More recently, GeoChat [26] proposed to adapt the LLaVA [34] model to remote sensing data, while integrating special task tokens into the textual instructions. This improves the zero-shot performance across a broad set of tasks, including image and region captioning, VQA, scene classification, and grounding descriptions. Following this trend, similar approaches such as SkyEyeGPT [68], LHRS-Bot [39], and VHM [40] employ comparable instruction-following architectures. The most recent efforts, such as EarthGPT [74] and EarthDial [51], introduce multi-modal models and datasets that fuse multiple data forms, such as optical, SAR, and multi-spectral.

While these works show the promise of grounded conversation in remote sensing, they often struggle to ground objects accurately due to their reliance on encoding location context into text. In our work, we address this limitation by introducing a dual approach that jointly models both language and bounding box spaces, enabling more precise and interpretable grounding in remote sensing data.

## 3. Method

### 3.1. Problem formulation

The basic framework for grounded multi-modal learning on Earth observation data can be specified as follows:

$$\mathcal{M}_{\text{vlm}} : (\mathbf{x}, \mathbf{q}) \mapsto \mathbf{a}, \quad (1)$$

where the vision-language model  $\mathcal{M}_{\text{vlm}}$  processes a satellite image  $\mathbf{x} \in \mathbb{R}^{H \times W \times 3}$  and a text query  $\mathbf{q} \in \mathcal{V}^{N_q}$  to produce a textual response  $\mathbf{a} \in \mathcal{V}^{N_a}$ . We commonly assume that addressing  $\mathbf{q}$  requires reasoning about the content of the image  $\mathbf{x}$ . Here,  $W, H \in \mathbb{N}$  denote the spatial size of the input image, while  $N_q, N_a \in \mathbb{N}$  correspond to the sequence length of  $\mathbf{q}$  and  $\mathbf{a}$ , respectively. Both sequences specify tokens from a common vocabulary:

$$\mathcal{V} := \mathcal{T} \cup \mathcal{S} := \{\mathbf{t}_1, \dots, \mathbf{t}_{|\mathcal{T}|}\} \cup \{\langle bos \rangle, \langle eos \rangle, \langle pad \rangle\}, \quad (2)$$

which comprises text tokens  $\mathcal{T}$ , as well as special control tokens  $\mathcal{S}$ , such as the beginning-of-sequence token  $\langle bos \rangle$ , the end-of-sequence token  $\langle eos \rangle$ , and the padding token  $\langle pad \rangle$ .

**Motivation.** Standard grounding techniques for vision-language models on Earth observation data embed location context within text representations, to allow implicit learning of spatial relations through next-token prediction. However, this method lacks explicit geometric modeling, which hinders the ability of the model to capture the precise spatial layout of satellite images.

To address this limitation, we modify the framework to incorporate explicit geometric reasoning. Rather than relying on implicit location information via next-token prediction, we introduce a grounding mechanism to predict bounding box locations directly. This model is defined as follows:

$$\mathcal{M}_{\text{loc}} : (\mathbf{x}, \mathbf{q}) \mapsto (\mathbf{a}, \ell). \quad (3)$$

Besides mapping an image  $\mathbf{x} \in \mathbb{R}^{H \times W \times 3}$  and text query  $\mathbf{q} \in \mathcal{V}^{N_q}$  to a reply  $\mathbf{a} \in \mathcal{V}^{N_a}$ , this localization model  $\mathcal{M}_{\text{loc}}$

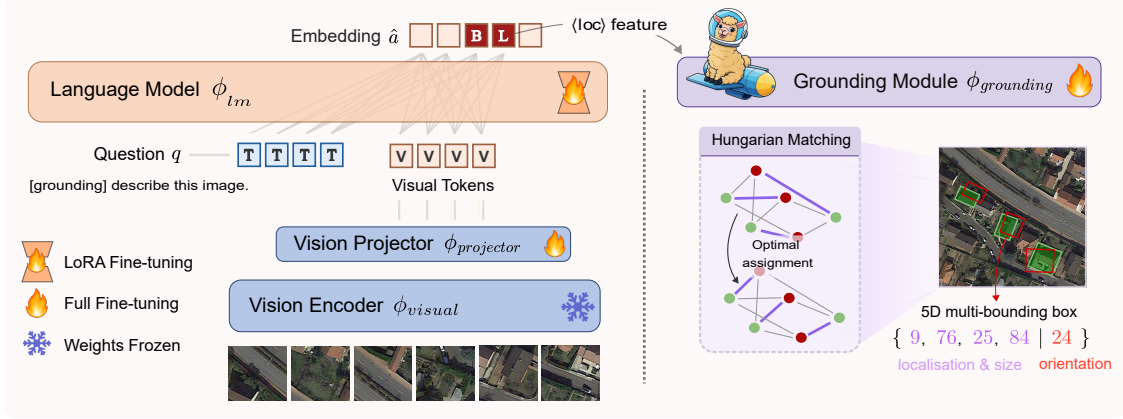


Figure 3. **Method overview.** We summarize the different components of our model. Visual inputs are encoded using a frozen vision backbone,  $\phi_{\text{visual}}$ , and a trainable adapter  $\phi_{\text{projector}}$ . The extracted vision tokens are then concatenated with the user query and passed to the language model  $\phi_{\text{lm}}$  based on LLaVA [34], which we finetune by applying LoRA [22]. The model’s response contains both standard text tokens and occasional  $\langle bb \rangle$  and  $\langle loc \rangle$  tokens, see Sec. 3.2 for more details. Any resulting  $\langle loc \rangle$  feature embeddings are passed to the grounding module  $\phi_{\text{grounding}}$  which produces the final bounding box predictions and matches them by using the Hungarian algorithm.

also directly predicts the bounding box locations  $\ell \in \mathbb{R}^{L \times 5}$ . Here,  $\ell$  represents coordinates of  $L \in \mathbb{N}$  different predicted bounding boxes, each fully specified by 5 parameters: 4 for the location (coordinates of the top left corner, bottom right corner) and 1 for the orientation (angle of rotation). We further append two additional special tokens to the vocabulary:

$$\bar{\mathcal{V}} := \mathcal{V} \cup \{\langle bb \rangle, \langle loc \rangle\}, \quad (4)$$

denoting bounding boxes  $\langle bb \rangle$  and location  $\langle loc \rangle$  tokens, respectively. In Fig. 2, we visualize our bounding box representation for a given query in comparison to the standard text-based format. We describe in Sec. 3.2 how integrating these tokens enables structured visual grounding in our model.

To facilitate gradient-based learning, we define  $\mathcal{M}_{\text{loc}}$  with a differentiable mapping from image  $\hat{\mathbf{x}}$  and text  $\hat{\mathbf{q}}$  embeddings<sup>1</sup> to locations  $\ell$ . The model thus optimizes the language output and bounding box locations simultaneously, enabling it to reason about how geometric details correspond to textual cues.

### 3.2. Structured visual grounding

The vocabulary space of possible output tokens in Eq. (4) includes text tokens, control tokens  $\langle bos \rangle$ ,  $\langle eos \rangle$ ,  $\langle pad \rangle$ , and two additional special tokens  $\langle bb \rangle$  and  $\langle loc \rangle$ . We now detail the latter two, which specify a grounding interface for regressing bounding box parameters in our model.

**Bounding box and location tokens.** By convention, the two special bounding box tokens always appear in sequence

<sup>1</sup>By convention, we denote  $\hat{\mathbf{x}}$  and  $\hat{\mathbf{q}}$  for the embedded features in latent space corresponding to data instances such as images  $\mathbf{x}$  and text  $\mathbf{q}$ .

$\langle bb \rangle \langle loc \rangle$  in a given text sample. They serve two distinct purposes:  $\langle bb \rangle$  indicates that the model produces a bounding box as part of the current predicted sentence.  $\langle loc \rangle$  then provides latent features for the corresponding bounding box parameters (*i.e.*, its location and orientation). The design choice of introducing two separate tokens  $\langle bb \rangle$  and  $\langle loc \rangle$  ensures a clear separation of responsibilities, and avoids sharing the capacity of a single embedding vector between these tasks. Our ablation study in Tab. 4 confirms this design is crucial, demonstrating that the separated tokens achieve an improved performance compared to a single-token approach.

**Training.** During training, our model naturally produces bounding box tokens  $\mathbf{a}_t = \langle bb \rangle$  as part of the output sequence  $\mathbf{a} \in \bar{\mathcal{V}}^{N_a}$  via standard next-token prediction. In contrast, the location tokens  $\langle loc \rangle$  are masked out when computing the cross-entropy token loss<sup>2</sup>, analogous to padding tokens  $\langle pad \rangle$ . Instead, we pass the latent embeddings  $\hat{\mathbf{a}}_t \in \mathbb{R}^D$  associated with  $\mathbf{a}_t = \langle loc \rangle$  with latent embedding dimensionality  $D$  to a separate grounding module:

$$\phi_{\text{grounding}} : \begin{cases} \mathbb{R}^{L \times D} \rightarrow \mathbb{R}^{L \times 5} \\ \{\hat{\mathbf{a}}_t \in \mathbb{R}^D | \mathbf{a}_t = \langle loc \rangle\} \mapsto \ell \end{cases} \quad (5)$$

which predicts the bounding box coordinates  $\ell \in \mathbb{R}^{L \times 5}$ . In practice  $\phi_{\text{grounding}}$  is defined as a shallow MLP. The goal is to accurately predict the location of a specific object while interfacing the VLM’s language capabilities. We provide a graphical representation of our approach in Fig. 3. To

<sup>2</sup>Since  $\langle loc \rangle$  always appears right after  $\langle bb \rangle$  in a fully deterministic manner, it carries no information for next-token prediction (zero entropy).

finetune the model (see Sec. 3.3 for details), we optimize for both the language modeling task and the location task simultaneously:

$$\mathcal{L} = \lambda_{\text{text}} \mathcal{L}_{\text{CE}} + \lambda_{\text{bb}} \mathcal{L}_{\text{ground}}, \quad (6)$$

where  $\mathcal{L}_{\text{CE}}$  represents the cross-entropy loss for predicting the next token in the sequence,  $\mathcal{L}_{\text{ground}}$  is the grounding loss for regressing the bounding box coordinates, and  $\lambda_{\text{text}}, \lambda_{\text{bb}}$  are hyperparameters indicating their relative weights.

Since the model may output the bounding boxes  $\ell$  of multiple objects in arbitrary order, we enforce permutation invariance of  $\mathcal{L}_{\text{ground}}$  by computing a bipartite matching of  $\ell \in \mathbb{R}^{L \times 5}$  to the reference bounding box coordinates  $\mathbf{k} \in \mathbb{R}^{K \times 5}$ . Following standard practice in the literature [7, 52], this is formulated as a linear sum assignment:

$$\mathcal{L}_{\text{ground}}(\ell, \mathbf{k}) := \min_{\rho \in \mathcal{P}_{L,K}} \sum_{i=1}^L \sum_{j=1}^K \rho_{i,j} \|\ell_i - \mathbf{k}_j\|^2, \quad (7)$$

which can be efficiently solved using the Hungarian algorithm [27]. Here,  $\rho \in \mathcal{P}_{L,K} \subset \{0,1\}^{L \times K}$  denotes a partial permutation matrix that defines an optimal one-to-one matching between a subset of the predicted and reference boxes, allowing for unmatched predictions or ground-truth boxes when their counts differ.

**Inference.** To produce an answer sequence  $(\mathbf{a}_t)_{1 \leq t \leq N_a}$  during inference, we apply standard next-token prediction in a greedy sampling scheme. When the model produces a  $\langle \text{bb} \rangle$  token, we append  $\langle \text{loc} \rangle$  immediately afterwards. Moreover, the corresponding embeddings  $\hat{\mathbf{a}}_t \in \mathbb{R}^D$  for occurrences of  $\mathbf{a}_t = \langle \text{loc} \rangle$  are again passed to the grounding module  $\phi_{\text{grounding}}$  to predict 5-D bounding box parameter vectors. We provide a detailed description of our inference-time sampling algorithm in Appendix Sec. 7.

### 3.3. Implementation details

**Datasets.** Our main motivation is to finetune a generalist VLM that can be applied to different downstream visual perception tasks on remote sensing data. To this end, we utilize the GeoChat [26] and EarthDial [51] multi-modal datasets for finetuning our model. These datasets are aggregated from a variety of sources [14, 36, 46] for a range of tasks, including visual question answering (VQA), grounding description, detailed description, multi-turn conversation, region captioning, referring expression, and scene classification. Training on such a large suite of problems helps to instill a holistic understanding of relevant data instances into the model.

We preprocess each training sample by normalizing the 5 entries of the bounding box parameters to the interval  $[0, 100]$ . We further adapt the considered datasets by inserting the special tokens for bounding boxes  $\langle \text{bb} \rangle$  and locations  $\langle \text{loc} \rangle$  required by our approach.

**Architecture details.** Our model’s core architecture consists of a pretrained, frozen ViT visual encoder [45] and a language decoder. We also employ a 2-layer MLP projector, which is responsible for mapping our location embeddings ( $\hat{\mathbf{a}}_t \in \mathbb{R}^D$  associated with  $\mathbf{a}_t = \langle \text{loc} \rangle$ ) for grounding, as detailed in Sec. 3.2. To ensure a fair comparison with the GeoChat and EarthDial baseline approaches, our experiments use the same respective language decoder. Specifically, we use the Vicuna-v1.5 [15] model for the GeoChat comparison and the Phi-3-mini [1] model for EarthDial. For data processing on GeoChat, we use 504x504 image inputs with interpolated positional embeddings. For the EarthDial benchmark, we employ the multi-modal (i.e., multi-spectral, SAR, temporal) and multi-resolution data fusion strategy detailed in [51]. Unless stated otherwise, all following experiments use this EarthDial setting.

## 4. Experiments

We evaluate our method on several tasks, including referring expression detection, grounding description, and two visual question answering benchmarks. For several of these tasks, we also assess generalization to different datasets in a zero-shot manner.

### 4.1. Grounding and referring expression detection

**Dataset.** We evaluate our model on the GeoChat [26] test set, and further assess zero-shot performance on NWPU VHR-10 [13], Swimming Pool [51] and Urban Tree Crown Detection [66]. These four datasets comprise 7,593, 1,601, 5,697, and 1,279 instances, respectively, all of which feature a mix of single and multi-object queries. The benchmarks differ in their task definition: by design, GeoChat categorizes queries into distinct “Grounding” and “Referring” groups based on object attributes, while the remaining three benchmarks feature a single, holistic “Referring” task.

**Task.** The objective here is to precisely localize the visual objects specified by a text query  $\mathbf{q}$  within an input image  $\mathbf{x}$ , outputting their corresponding bounding box locations  $\ell$ . The queries in the considered benchmarks refer to diverse objects of interest, including storage tanks, cars, and airplanes, swimming pools, as well as larger objects such as football fields and bridges. We follow the prior convention [26, 51] of reporting the  $\text{acc}@0.5$  score as the main evaluation score, defined as the fraction of correct predictions with an IoU score larger than 0.5.

**Discussion.** We report quantitative results on the GeoChat test set in Tab. 1. The table details two finetuning experiments. In both cases, our method demonstrates clear performance gains: on the GeoChat dataset, we achieve 24.5% accuracy, outperforming the strongest baseline EarthDial



Model	Object Size			Grounding			Referring			Overall
	Small	Medium	Large	Single	Multi	Avg.	Single	Multi	Avg.	
<i>Finetuned on GeoChat</i>										
LHRS-Bot [39]	0.2	1.9	9.4	18.6	3.8	5.2	3.2	1.2	2.5	2.7
MiniGPTv2 [10]	1.7	9.9	21.9	9.1	3.6	2.6	–	–	8.2	7.6
GeoChat [26]	2.9	13.6	21.7	16.0	4.3	11.8	–	–	10.5	10.6
TeoChat [24]	2.3	11.6	29.0	32.2	9.3	10.6	15.1	4.8	11.2	11.1
InternVL2-4B [12]	7.0	22.3	33.5	24.4	11.5	12.5	25.6	8.4	18.9	18.2
EarthDial [51]	6.8	23.8	32.9	25.9	13.0	13.9	26.0	8.4	19.3	18.6
Ours	9.1	30.5	44.1	37.3	17.4	18.7	33.8	10.0	25.1	24.5
<i>Finetuned on EarthDial</i>										
EarthDial [51]	11.4	31.7	39.1	28.2	18.1	18.8	34.4	12.0	25.8	25.0
Ours	11.5	36.6	57.5	32.0	29.1	29.5	37.5	10.9	31.3	31.2

Table 1. **Quantitative results for visual grounding and referring on the GeoChat benchmark.** We report the accuracy (%) score. Performance is broken down by object size (Small, Medium, Large) and task type. For the Grounding and Referring tasks, we evaluate performance on prompts with single vs. multiple objects. The Avg. column shows the mean score for each task category.

Model	NWPU VHR-10 [13]					Swimming Pool Dataset [51]					Urban Tree Crown Detection [66]				
	Object Size			Referring		Object Size			Referring		Object Size			Referring	
	Small	Medium	Large	Single	Multi	Small	Medium	Large	Single	Multi	Small	Medium	Large	Single	Multi
GeoChat [26]	2.5	3.2	14.7	13.2	1.9	-	3.1	7.3	1.2	0.6	-	1.8	8.9	2.9	3.1
InternVL2-4B [12]	7.1	12.7	25.5	23.0	8.1	0.6	6.6	8.9	4.5	0.9	-	3.2	13.4	5.9	3.1
InternVL2-8B [12]	4.3	11.8	20.7	21.7	5.9	0.3	4.7	18.3	7.6	0.5	0.6	4.0	17.1	7.9	3.9
EarthDial [51]	11.7	14.2	23.1	25.4	8.9	1.0	7.4	24.9	8.4	1.0	<b>1.1</b>	<b>7.0</b>	<b>25.7</b>	<b>11.1</b>	<b>6.7</b>
Ours	<b>14.6</b>	<b>22.9</b>	<b>36.7</b>	<b>29.3</b>	<b>14.9</b>	<b>2.9</b>	<b>8.4</b>	<b>27.2</b>	<b>9.6</b>	<b>3.0</b>	0.3	4.9	15.4	6.1	6.1

Table 2. **Quantitative results for zero-shot referring object detection.** We compare our model’s generalization performance against several baselines on three datasets: NWPU VHR-10 [13], Swimming Pool [51], and Urban Tree Crown Detection [66].

by 5.9%. When finetuning on the EarthDial dataset, our model improves the overall accuracy by a sizable margin of 6.2% ( $\hat{=}$  relative improvement of 24.8%). This robust performance further translates to the zero-shot setting shown in Tab. 2, where our model outperforms baseline methods on two out of three considered downstream tasks (NWPU VHR-10 and Swimming Pools), while remaining competitive on Tree Crown Detection. We further provide several qualitative examples in Fig. 4.

## 4.2. Grounding description

**Datasets.** We evaluate the grounding description capabilities of our model in a zero-shot setting on four benchmarks: HIT-UAV [53], NWPU VHR-10 [13], Swimming Pool [51], and UCAS-AOD [77]. These datasets cover diverse object categories and data types ranging from standard imagery to thermal data.

**Task.** Grounding description is a challenging task, where the model predicts both a natural language response  $a$  and corresponding bounding box locations  $\ell$ . This dual-output structure requires an integrated capacity for both high-level linguistic reasoning and precise localization. We evaluate

localization using the accuracy score analogous to our previous grounding experiments ( $\text{IoU} > 0.5$  and  $0.25$ ), and assess the text quality using ROUGE-1 (R-1), ROUGE-L (R-L), and METEOR (MT) scores.

**Discussion.** We provide quantitative comparisons for zero-shot grounding description in Tab. 3. Our model achieves the most consistent performance overall, while outperforming the baseline approaches on text-based metrics across all four benchmarks. This improvement is particularly notable on UCAS-AOD, where our model achieves a 35.4% R-1 score, a +14.2% absolute gain over the best baseline EarthDial.

## 4.3. Visual question answering

**Datasets.** We evaluate the performance of our method on visual question answering (VQA) for remote sensing using the HRBEN and LRBEN benchmarks [36]. Both datasets focus on answering natural language questions about the content of aerial images. On HRBEN, we provide comparisons on the default test set, which contains 62,554 question-answer pairs. All these evaluations are performed in a zero-shot manner, *i.e.*, without finetuning on HRBEN’s

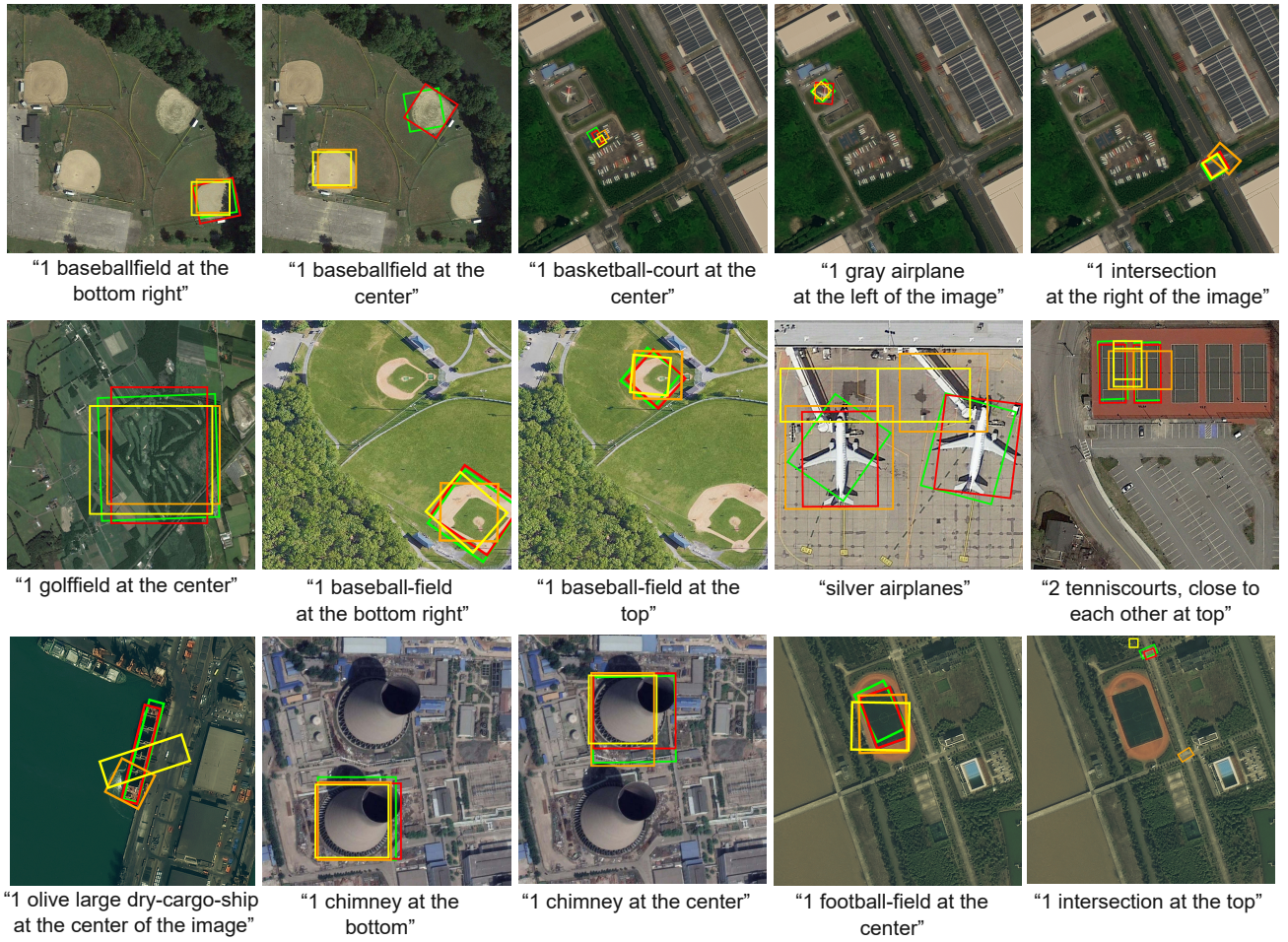


Figure 4. **Qualitative comparison for visual grounding.** These instances correspond to the quantitative results from Tab. 1. For each sample, we provide predictions by our approach in green, InternVL [12] in orange, and EarthDial [51] in yellow. The ground truth bounding boxes are shown in red.

Model	HIT-UAV [53]					NWPU VHR-10 [13]					Swimming Pool Dataset [51]					UCAS-AOD [77]				
	@0.5	@0.25	R-1	R-L	MT	@0.5	@0.25	R-1	R-L	MT	@0.5	@0.25	R-1	R-L	MT	@0.5	@0.25	R-1	R-L	MT
GPT-4o	0.1	0.7	14.2	10.6	7.2	0.7	6.1	14.7	10.8	9.4	0.1	1.2	12.9	10.1	7.8	0.1	1.3	14.7	11.1	6.0
InternVL2-4B [12]	0.6	6.4	28.1	27.7	24.0	10.6	29.9	30.7	29.1	21.9	0.8	4.2	28.3	28.1	24.6	4.6	31.8	21.0	20.0	11.6
GeoChat [26]	0.8	8.0	22.8	22.2	22.3	2.2	15.3	21.5	20.7	21.4	1.8	<b>8.8</b>	21.4	21.1	24.0	1.4	13.6	20.0	18.8	14.2
EarthDial [51]	<b>2.6</b>	13.9	28.3	28.1	22.2	17.1	<b>41.0</b>	27.0	26.3	23.1	<b>1.9</b>	7.4	29.7	29.3	22.8	<b>8.5</b>	<b>34.0</b>	21.2	20.3	13.0
<b>Ours</b>	1.7	<b>17.9</b>	<b>33.8</b>	<b>32.6</b>	<b>24.6</b>	<b>19.9</b>	37.8	<b>36.3</b>	<b>34.8</b>	<b>26.6</b>	1.2	7.7	<b>31.5</b>	<b>30.4</b>	<b>25.3</b>	2.7	20.8	<b>35.4</b>	<b>32.8</b>	<b>15.7</b>

Table 3. **Quantitative results for zero-shot grounding description.** We evaluate our model’s ability to generate both textual descriptions and corresponding bounding boxes for given text queries and images. Performance is reported with ROUGE-1 (R-1), ROUGE-L (R-L), METEOR (M-T) scores, and accuracy (%) for bounding box prediction (IoU > 0.5 and 0.25).

training set. In contrast, generalist approaches such as ours are implicitly finetuned on the LRBEN training set, since this is one of the datasets comprising the general instruction-tuning dataset GeoChat [26] ( $\sim 18.3\%$  of the training samples). Specialist methods such as RSGPT are finetuned on the training set of the specific benchmark to achieve an optimal performance [23].

**Tasks.** We consider two question types (presence, comparison) for HRBEN and three types (presence, comparison, rural/urban classification) for LRBEN, in alignment with prior work [23, 26, 39]. The goal of presence questions is classifying whether a specific instance is part of an image (e.g., “Is there a grass area on the right of a commercial building?”). Comparison questions require estimat-

Hungarian	With $\langle bb \rangle$	Small	Medium	Large	Grounding	Referring	Overall
✓		7.9	21.0	39.8	17.1	19.3	19.2
	✓	8.3	27.4	39.1	18.1	22.2	21.8
✓	✓	<b>9.1</b>	<b>30.5</b>	<b>44.1</b>	<b>18.7</b>	<b>25.1</b>	<b>24.5</b>

(a) Impact of Hungarian matching and  $\langle bb \rangle$ .

$\lambda_{bb}$	Small	Medium	Large	Grounding	Referring	Overall
5	9.1	28.1	42.6	20.0	23.3	23.0
10	<b>9.1</b>	<b>30.5</b>	<b>44.1</b>	18.7	<b>25.1</b>	<b>24.5</b>
20	8.7	27.0	43.0	<b>20.3</b>	23.0	22.7

(b) Impact of grounding loss weight  $\lambda_{bb}$ .

Table 4. **Ablation study.** (a) We assess the role of the Hungarian matching in our grounding module. Moreover, we evaluate how our two-token design compares to a variant where we remove  $\langle bb \rangle$  and merge both tasks into a single token. (b) We further quantify the impact of the loss weight  $\lambda_{bb}$  on the visual grounding accuracy. Specifically, we analyze the impact on small, medium, and large object detection, as well as grounding and referring tasks. These results confirm the necessity of all components for an optimal performance.

Model	Pres.	Comp.	R/U	Avg.
<i>Zero-shot</i>				
Qwen-VL [5]	38.6	67.6	<b>61.0</b>	55.4
LLaVA-1.5 [33]	<b>55.5</b>	<b>68.2</b>	59.0	<b>62.8</b>
MiniGPTv2 [10]	55.2	55.5	39.0	55.0
<i>Specialist</i>				
RSVQA	87.5	81.5	90.0	86.3
RSGPT	<b>91.2</b>	<b>91.7</b>	<b>94.0</b>	<b>92.3</b>
<i>Generalist</i>				
LHRs-Bot [39]	88.5	90.0	89.1	89.4
GeoChat [26]	91.1	90.3	<b>94.0</b>	90.7
EarthDial [51]	<b>92.6</b>	<b>92.7</b>	<b>94.0</b>	<b>92.7</b>
Ours	91.7	92.6	93.0	92.2

Table 5. **Quantitative VQA results on HRBEN (left) and LRBEN (right).** On HRBEN, we evaluate our method in a zero-shot setting; while not specifically designed for this task, our method achieves the best overall performance compared to the considered baselines. The LRBEN evaluation compares three classes of methods: zero-shot, specialist (finetuned for this benchmark), and generalist (finetuned for multiple tasks). The columns report the accuracy for Presence, Comparison, and Rural/Urban question types, along with the average scores.

ing and contrasting two quantities (e.g., “Are there more water areas than commercial buildings?” or “Is the number of buildings equal to the number of roads?”). While presence questions primarily rely on object detection, comparison questions involve both object detection and numerical reasoning, making them inherently more challenging. Rural/urban classification predicts whether an area is urban or rural based on visual criteria such as building density (e.g., “Is this a rural or urban area?”), thus involving scene-level classification rather than object detection.

**Discussion.** In Tab. 5, we provide quantitative comparisons for both HRBEN and LRBEN. Our method achieves the best overall zero-shot generalization performance on HRBEN, while obtaining the second best performance after EarthDial [51] on LRBEN among generalist methods. While LRBEN is fairly saturated and the gap is small (−0.5% average accuracy), our method advances the state-of-the-art on HRBEN by a sizable margin of +2.5%, hence obtaining the best overall performance across all settings. Both approaches advance the state-of-the-art while matching specialist approaches, even slightly outperforming RS-GPT [23] on the “presence” and “comparison” questions.

#### 4.4. Ablation study

In Sec. 3.2, we introduce our dual visual grounding module, combining next-token prediction and bounding box detection. Here, we assess the impact of key components on the overall performance, see Tab. 4 for a summary. We conduct all ablations using the GeoChat setting.

**Two token design.** We compare our two-token design to a setup where we do not use the  $\langle bb \rangle$  token, and instead merge both responsibilities (predicting bounding boxes in the response, producing bounding box coordinates) into a single  $\langle loc \rangle$  token. As shown in Tab. 4a, this leads to a decreased performance, since it requires sharing the capacity of a single embedding vector between these tasks.

**Hungarian matching.** We further investigate the role of the Hungarian algorithm in bounding box regression. As shown in the second row of Tab. 4a, disabling Hungarian matching leads to reduced overall performance (24.5% vs. 21.8%). This underscores the importance of permutation-invariant matching for precise localization.

**Loss weight.** Lastly, we explore the effect of different values for  $\lambda_{bb}$ , which specifies the weight of the grounding loss  $\mathcal{L}_{\text{ground}}$  defined in Eq. (6). We find that setting  $\lambda_{bb} = 10$  yields the best overall performance, see Tab. 4b. Lowering  $\lambda_{bb}$  to 5, or increasing to 20 reduces the accuracy, particularly in medium and large object categories.

#### 5. Conclusion

We present *SATGround*, a novel approach for spatially-aware visual grounding in remote sensing. Our method integrates multi-modal learning with a specialized localization mechanism, enabling precise alignment of textual queries with visual semantics in satellite imagery. By finetuning a generalist vision-language model with specialized control tokens and a custom grounding module, we bridge the gap between language and spatial reasoning. Our experiments demonstrate that our model outperforms existing techniques across multiple benchmarks, including referring expression detection, grounding description, and visual question answering. Notably, we achieve a significant 24.8% relative improvement in visual grounding accuracy over prior methods, underscoring the effectiveness of our structured localization approach for real-world satellite data analysis.



## References

- [1] Marah Abdin et al. Phi-3 technical report: A highly capable language model locally on your phone. Technical report, 2024. [5](#)
- [2] Josh Achiam, Steven Adler, Sandhini Agarwal, Lama Ahmad, Ilge Akkaya, Florencia Leoni Aleman, Diogo Almeida, Janko Altenschmidt, Sam Altman, Shyamal Anadkat, et al. Gpt-4 technical report. *arXiv:2303.08774*, 2023. [2](#)
- [3] Konstantinos Panagiotis Alexandridis, Ismail Elezi, Jiankang Deng, Anh Nguyen, and Shan Luo. Fractal calibration for long-tailed object detection. In *CVPR*, 2025. [2](#)
- [4] Josef Aschbacher. Esa’s earth observation strategy and copernicus. *Satellite earth observations and their impact on society and policy*, 2017. [1](#)
- [5] Jinze Bai, Shuai Bai, Shusheng Yang, Shijie Wang, Sinan Tan, Peng Wang, Junyang Lin, Chang Zhou, and Jingren Zhou. Qwen-vl: A frontier large vision-language model with versatile abilities. *arXiv:2308.12966*, 2023. [8](#)
- [6] Yakoub Bazi, Mohamad Mahmoud Al Rahhal, Mohamed Lamine Mekhalfi, Mansour Abdulaziz Al Zuair, and Farid Melgani. Bi-modal transformer-based approach for visual question answering in remote sensing imagery. *IEEE Transactions on Geoscience and Remote Sensing*, 2022. [3](#)
- [7] Nicolas Carion, Francisco Massa, Gabriel Synnaeve, Nicolas Usunier, Alexander Kirillov, and Sergey Zagoruyko. End-to-end object detection with transformers. In *ECCV*, 2020. [5](#)
- [8] Soravit Changpinyo, Piyush Sharma, Nan Ding, and Radu Soricut. Conceptual 12m: Pushing web-scale image-text pre-training to recognize long-tail visual concepts. In *CVPR*, 2021. [2](#)
- [9] Christel Chappuis, Valérie Zermatten, Sylvain Lobry, Bertrand Le Saux, and Devis Tuia. Prompt-rsvqa: Prompting visual context to a language model for remote sensing visual question answering. In *CVPR*, 2022. [3](#)
- [10] Jun Chen, Deyao Zhu, Xiaoqian Shen, Xiang Li, Zechun Liu, Pengchuan Zhang, Raghuraman Krishnamoorthi, Vikas Chandra, Yunyang Xiong, and Mohamed Elhoseiny. Minigt-v2: large language model as a unified interface for vision-language multi-task learning. *arXiv:2310.09478*, 2024. [6](#), [8](#)
- [11] Keqin Chen, Zhao Zhang, Weili Zeng, Richong Zhang, Feng Zhu, and Rui Zhao. Shikra: Unleashing multimodal llm’s referential dialogue magic. *arXiv:2306.15195*, 2023. [2](#)
- [12] Zhe Chen, Jiannan Wu, Wenhai Wang, Weijie Su, Guo Chen, Sen Xing, Muyan Zhong, Qinglong Zhang, Xizhou Zhu, Lewei Lu, et al. Internvl: Scaling up vision foundation models and aligning for generic visual-linguistic tasks. In *CVPR*, 2024. [1](#), [6](#), [7](#)
- [13] Gong Cheng, Junwei Han, Peicheng Zhou, and Lei Guo. Multi-class geospatial object detection and geographic image classification based on collection of part detectors. *ISPRS Journal of Photogrammetry and Remote Sensing*, 98: 119–132, 2014. [2](#), [5](#), [6](#), [7](#)
- [14] Gong Cheng, Junwei Han, and Xiaoqiang Lu. Remote sensing image scene classification: Benchmark and state of the art. *Proceedings of the IEEE*, 2017. [5](#)
- [15] Wei-Lin Chiang, Zhuohan Li, Zi Lin, Ying Sheng, Zhanghao Wu, Hao Zhang, Lianmin Zheng, Siyuan Zhuang, Yonghao Zhuang, Joseph E Gonzalez, et al. Vicuna: An open-source chatbot impressing gpt-4 with 90%\* chatgpt quality. See <https://vicuna.lmsys.org> (accessed 14 April 2023), 2023. [2](#), [5](#)
- [16] Yu Du, Fangyun Wei, Zihe Zhang, Miaoqing Shi, Yue Gao, and Guoqi Li. Learning to prompt for open-vocabulary object detection with vision-language model. In *CVPR*, 2022. [2](#)
- [17] Ismail Elezi, Jenny Seidenschwarz, Laurin Wagner, Sebastian Vascon, Alessandro Torcinovich, Marcello Pelillo, and Laura Leal-Taixé. The group loss++: A deeper look into group loss for deep metric learning. *TPAMI*, 2023. [2](#)
- [18] Vladimir Fomenko, Ismail Elezi, Deva Ramanan, Laura Leal-Taixé, and Aljosa Osep. Learning to discover and detect objects. In *NeurIPS*, 2022. [2](#)
- [19] Muhammed Goktepe, Amir hossein Shamseddin, Erencan Uysal, Javier Muñelo Monteagudo, Lukas Drees, Aysim Toker, Senthod Asseng, and Malte von Bloh. Ecomapper: Generative modeling for climate-aware satellite imagery. In *Forty-second International Conference on Machine Learning*, 2025. [2](#)
- [20] Xiuye Gu, Tsung-Yi Lin, Weicheng Kuo, and Yin Cui. Open-vocabulary object detection via vision and language knowledge distillation. *ICLR*, 2022. [2](#)
- [21] Ritwik Gupta, Bryce Goodman, Nirav Patel, Ricky Hosfelt, Sandra Sajeev, Eric Heim, Jigar Doshi, Keane Lucas, Howie Choset, and Matthew Gaston. Creating xbd: A dataset for assessing building damage from satellite imagery. In *CVPRW*, 2019. [2](#)
- [22] Edward J Hu, Yelong Shen, Phillip Wallis, Zeyuan Allen-Zhu, Yuanzhi Li, Shean Wang, Lu Wang, Weizhu Chen, et al. Lora: Low-rank adaptation of large language models. In *ICLR*, 2022. [4](#)
- [23] Yuan Hu, Jianlong Yuan, Congcong Wen, Xiaonan Lu, and Xiang Li. Rsgpt: A remote sensing vision language model and benchmark. *arXiv:2307.15266*, 2023. [3](#), [7](#), [8](#)
- [24] Jeremy Andrew Irvin, Emily Ruoyu Liu, Joyce Chuyi Chen, Ines Dormoy, Jinyoung Kim, Samar Khanna, Zhuo Zheng, and Stefano Ermon. TeoChat: A large vision-language assistant for temporal earth observation data. In *ICLR*, 2025. [6](#)
- [25] Chao Jia, Yinfei Yang, Ye Xia, Yi-Ting Chen, Zarana Parekh, Hieu Pham, Quoc Le, Yun-Hsuan Sung, Zhen Li, and Tom Duerig. Scaling up visual and vision-language representation learning with noisy text supervision. In *ICML*, 2021. [2](#)
- [26] Kartik Kuckreja, Muhammad Sohail Danish, Muzammal Naseer, Abhijit Das, Salman Khan, and Fahad Shahbaz Khan. GeoChat: Grounded large vision-language model for remote sensing. In *CVPR*, 2024. [2](#), [3](#), [5](#), [6](#), [7](#), [8](#)
- [27] Harold W Kuhn. The hungarian method for the assignment problem. *Naval research logistics quarterly*, 1955. [5](#)
- [28] Xin Lai, Zhuotao Tian, Yukang Chen, Yanwei Li, Yuhui Yuan, Shu Liu, and Jiaya Jia. Lisa: Reasoning segmentation via large language model. In *CVPR*, 2024. [2](#)
- [29] Liunan Harold Li, Pengchuan Zhang, Haotian Zhang, Jianwei Yang, Chunyuan Li, Yiwu Zhong, Lijuan Wang, Lu

- Yuan, Lei Zhang, Jenq-Neng Hwang, et al. Grounded language-image pre-training. In *CVPR*, 2022. 2
- [30] Xiang Li, Congcong Wen, Yuan Hu, and Nan Zhou. Rs-clip: Zero shot remote sensing scene classification via contrastive vision-language supervision. *International Journal of Applied Earth Observation and Geoinformation*, 2023. 3
- [31] Xiang Li, Congcong Wen, Yuan Hu, Zhenghang Yuan, and Xiao Xiang Zhu. Vision-language models in remote sensing: Current progress and future trends. *IEEE Geoscience and Remote Sensing Magazine*, 2024. 3
- [32] Tsung-Yi Lin, Michael Maire, Serge Belongie, James Hays, Pietro Perona, Deva Ramanan, Piotr Dollár, and C Lawrence Zitnick. Microsoft coco: Common objects in context. In *ECCV*, 2014. 2
- [33] Haotian Liu, Chunyuan Li, Yuheng Li, and Yong Jae Lee. Improved baselines with visual instruction tuning. In *CVPR*, 2024. 8
- [34] Haotian Liu, Chunyuan Li, Qingyang Wu, and Yong Jae Lee. Visual instruction tuning. In *NeurIPS*, 2024. 2, 3, 4
- [35] Shilong Liu, Hao Cheng, Haotian Liu, Hao Zhang, Feng Li, Tianhe Ren, Xueyan Zou, Jianwei Yang, Hang Su, Jun Zhu, et al. Llava-plus: Learning to use tools for creating multimodal agents. In *ECCV*, 2024. 2
- [36] Sylvain Lobry, Diego Marcos, Jesse Murray, and Devis Tuia. Rsvqa: Visual question answering for remote sensing data. *IEEE Transactions on Geoscience and Remote Sensing*, 2020. 2, 5, 6
- [37] Jiasen Lu, Dhruv Batra, Devi Parikh, and Stefan Lee. Vilbert: Pretraining task-agnostic visiolinguistic representations for vision-and-language tasks. *NeurIPS*, 32, 2019. 2
- [38] Matthias Minderer, Alexey Gritsenko, Austin Stone, Maxim Neumann, Dirk Weissenborn, Alexey Dosovitskiy, Aravindh Mahendran, Anurag Arnab, Mostafa Dehghani, Zhuoran Shen, et al. Simple open-vocabulary object detection. In *ECCV*, 2022. 2
- [39] Dilxat Muhtar, Zhenshi Li, Feng Gu, Xueliang Zhang, and Pengfeng Xiao. Lhrs-bot: Empowering remote sensing with vgi-enhanced large multimodal language model. In *ECCV*, 2024. 2, 3, 6, 7, 8
- [40] Chao Pang, Jiang Wu, Jiayu Li, Yi Liu, Jiaying Sun, Weijia Li, Xingxing Weng, Shuai Wang, Litong Feng, Gui-Song Xia, et al. H2rsvlm: Towards helpful and honest remote sensing large vision language model. *CoRR*, 2024. 2, 3
- [41] Baolin Peng, Chunyuan Li, Pengcheng He, Michel Galley, and Jianfeng Gao. Instruction tuning with gpt-4. *arXiv:2304.03277*, 2023. 2
- [42] Zhiliang Peng, Wenhui Wang, Li Dong, Yaru Hao, Shaohan Huang, Shuming Ma, Qixiang Ye, and Furu Wei. Grounding multimodal large language models to the world. In *ICLR*, 2024. 2
- [43] Bryan A Plummer, Liwei Wang, Chris M Cervantes, Juan C Caicedo, Julia Hockenmaier, and Svetlana Lazebnik. Flickr30k entities: Collecting region-to-phrase correspondences for richer image-to-sentence models. In *ICCV*, 2015. 2
- [44] Chunping Qiu, Anzhu Yu, Xiaodong Yi, Naiyang Guan, Dianxi Shi, and Xiaochong Tong. Open self-supervised features for remote-sensing image scene classification using very few samples. *IEEE Geoscience and Remote Sensing Letters*, 2022. 3
- [45] Alec Radford, Jong Wook Kim, Chris Hallacy, Aditya Ramesh, Gabriel Goh, Sandhini Agarwal, Girish Sastry, Amanda Askell, Pamela Mishkin, Jack Clark, et al. Learning transferable visual models from natural language supervision. In *ICML*, 2021. 2, 5
- [46] Maryam Rahnemoonfar, Tashnim Chowdhury, Argho Sarkar, Debvrat Varshney, Masoud Yari, and Robin Robertson Murphy. Floodnet: A high resolution aerial imagery dataset for post flood scene understanding. *IEEE Access*, 2021. 5
- [47] Christoph Schuhmann, Romain Beaumont, Richard Vencu, Cade Gordon, Ross Wightman, Mehdi Cherti, Theo Coombes, Aarush Katta, Clayton Mullis, Mitchell Wortsman, et al. Laion-5b: An open large-scale dataset for training next generation image-text models. In *NeurIPS*, 2022. 2
- [48] Eli Schwartz, Leshem Choshen, Joseph Shtok, Sivan Doveh, Leonid Karlinsky, and Assaf Arbelle. Numerologic: Number encoding for enhanced llms’ numerical reasoning. In *EMNLP*, 2024. 2
- [49] Ruoqi Shen, Sébastien Bubeck, Ronen Eldan, Yin Tat Lee, Yuanzhi Li, and Yi Zhang. Positional description matters for transformers arithmetic. *arXiv:2311.14737*, 2023.
- [50] Aaditya K Singh and DJ Strouse. Tokenization counts: the impact of tokenization on arithmetic in frontier llms. *arXiv:2402.14903*, 2024. 2
- [51] Sagar Soni, Akshay Dudhane, Hiyam Debary, Mustansar Fiaz, Muhammad Akhtar Munir, Muhammad Sohail Danish, Paolo Fraccaro, Campbell D Watson, Levent J Klein, Fahad Shahbaz Khan, and Salman Khan. Earthdial: Turning multi-sensory earth observations to interactive dialogues. In *CVPR*, 2025. 1, 2, 3, 5, 6, 7, 8
- [52] Russell Stewart, Mykhaylo Andriluka, and Andrew Y Ng. End-to-end people detection in crowded scenes. In *CVPR*, 2016. 5
- [53] Jiashun Suo, Tianyi Wang, Xingzhou Zhang, Haiyang Chen, Wei Zhou, and Weisong Shi. Hit-uav: A high-altitude infrared thermal dataset for unmanned aerial vehicle-based object detection. *Scientific Data*, 10(1):227, 2023. 6, 7
- [54] Rohan Taori, Ishaan Gulrajani, Tianyi Zhang, Yann Dubois, Xuechen Li, Carlos Guestrin, Percy Liang, and Tatsunori B Hashimoto. Stanford alpaca: an instruction-following llama model (2023). URL [https://github.com/tatsu-lab/stanford\\_alpaca](https://github.com/tatsu-lab/stanford_alpaca), 1(9), 2023. 2
- [55] Aysim Toker, Qunjie Zhou, Maxim Maximov, and Laura Leal-Taixe. Coming down to earth: Satellite-to-street view synthesis for geo-localization. In *Proceedings of the IEEE/CVF Conference on Computer Vision and Pattern Recognition (CVPR)*, 2021. 2
- [56] Aysim Toker, Lukas Kondmann, Mark Weber, Marvin Eisenberger, Andres Camero, Jingliang Hu, Ariadna Pregel Hoderlein, Caglar Senaras, Timothy Davis, Daniel Cremers, Giovanni Marchisio, Xiaoxiang Zhu, and Laura Leal-Taixe. Dynamicearthnet: Daily multi-spectral satellite dataset for semantic change segmentation. In *Proceedings of the IEEE/CVF Conference on Computer Vision and Pattern Recognition (CVPR)*, 2022. 2

- [57] Aysim Toker, Marvin Eisenberger, Daniel Cremers, and Laura Leal-Taix'e. Satsynth: Augmenting image-mask pairs through diffusion models for aerial semantic segmentation. *2024 IEEE/CVF Conference on Computer Vision and Pattern Recognition (CVPR)*, 2024. 2
- [58] Hugo Touvron, Thibaut Lavril, Gautier Izacard, Xavier Martinet, Marie-Anne Lachaux, Timothée Lacroix, Baptiste Rozière, Naman Goyal, Eric Hambro, Faisal Azhar, et al. Llama: Open and efficient foundation language models. *arXiv:2302.13971*, 2023. 2
- [59] Weihang Wang, Qingsong Lv, Wenmeng Yu, Wenyi Hong, Ji Qi, Yan Wang, Junhui Ji, Zhuoyi Yang, Lei Zhao, Song XiXuan, Jiazheng Xu, Keqin Chen, Bin Xu, Juanzi Li, Yuxiao Dong, Ming Ding, and Jie Tang. CogVLM: Visual expert for pretrained language models. In *NeurIPS*, 2024. 2
- [60] Curtis E Woodcock, Richard Allen, Martha Anderson, Alan Belward, Robert Bindschadler, Warren Cohen, Feng Gao, Samuel N Goward, Dennis Helder, Eileen Helmer, et al. Free access to landsat imagery. *Science*, 2008. 1
- [61] Mengde Xu, Zheng Zhang, Fangyun Wei, Yutong Lin, Yue Cao, Han Hu, and Xiang Bai. A simple baseline for open-vocabulary semantic segmentation with pre-trained vision-language model. In *ECCV*, 2022. 2
- [62] Lewei Yao, Runhui Huang, Lu Hou, Guansong Lu, Minzhe Niu, Hang Xu, Xiaodan Liang, Zhenguo Li, Xin Jiang, and Chunjing Xu. FILIP: Fine-grained interactive language-image pre-training. In *ICLR*, 2022. 2
- [63] Haoxuan You, Haotian Zhang, Zhe Gan, Xianzhi Du, Bowen Zhang, Zirui Wang, Liangliang Cao, Shih-Fu Chang, and Yinfei Yang. Ferret: Refer and ground anything anywhere at any granularity. In *ICLR*, 2024. 2
- [64] Lu Yuan, Dongdong Chen, Yi-Ling Chen, Noel Codella, Xiyang Dai, Jianfeng Gao, Houdong Hu, Xuedong Huang, Boxin Li, Chunyuan Li, et al. Florence: A new foundation model for computer vision. *arXiv:2111.11432*, 2021. 2
- [65] Zhenghang Yuan, Lichao Mou, Qi Wang, and Xiao Xiang Zhu. From easy to hard: Learning language-guided curriculum for visual question answering on remote sensing data. *IEEE transactions on geoscience and remote sensing*, 2022. 3
- [66] Pedro Zamboni, José Marcato Junior, Jonathan de Andrade Silva, Gabriela Takahashi Miyoshi, Edson Takashi Matsubara, Keiller Nogueira, and Wesley Nunes Gonçalves. Benchmarking anchor-based and anchor-free state-of-the-art deep learning methods for individual tree detection in rgb high-resolution images. *Remote Sensing*, 2021. 5, 6
- [67] Xiaohua Zhai, Basil Mustafa, Alexander Kolesnikov, and Lucas Beyer. Sigmoid loss for language image pre-training. In *ICCV*, 2023. 2
- [68] Yang Zhan, Zhitong Xiong, and Yuan Yuan. Skyeyegpt: Unifying remote sensing vision-language tasks via instruction tuning with large language model. *ISPRS Journal of Photogrammetry and Remote Sensing*, 2025. 2, 3
- [69] Hao Zhang, Feng Li, Shilong Liu, Lei Zhang, Hang Su, Jun Zhu, Lionel Ni, and Heung-Yeung Shum. DINO: DETR with improved denoising anchor boxes for end-to-end object detection. In *ICLR*, 2023. 2
- [70] Hao Zhang, Hongyang Li, Feng Li, Tianhe Ren, Xueyan Zou, Shilong Liu, Shijia Huang, Jianfeng Gao, Leizhang, Chunyuan Li, et al. Llava-grounding: Grounded visual chat with large multimodal models. In *ECCV*, 2024. 2
- [71] Jingyi Zhang, Jiaxing Huang, Sheng Jin, and Shijian Lu. Vision-language models for vision tasks: A survey. *IEEE Transactions on Pattern Analysis and Machine Intelligence*, 2024. 2
- [72] Renrui Zhang, Ziyu Guo, Wei Zhang, Kunchang Li, Xupeng Miao, Bin Cui, Yu Qiao, Peng Gao, and Hongsheng Li. Pointclip: Point cloud understanding by clip. In *CVPR*, 2022. 2
- [73] Wei Zhang, Miaoxin Cai, Tong Zhang, Yin Zhuang, and Xuerui Mao. Earthgpt: A universal multimodal large language model for multisensor image comprehension in remote sensing domain. *IEEE Transactions on Geoscience and Remote Sensing*, 2024. 8
- [74] Wei Zhang, Miaoxin Cai, Tong Zhang, Yin Zhuang, and Xuerui Mao. Earthgpt: A universal multimodal large language model for multisensor image comprehension in remote sensing domain. *IEEE Transactions on Geoscience and Remote Sensing*, 2024. 3
- [75] Yang Zhao, Zhijie Lin, Daquan Zhou, Zilong Huang, Jiashi Feng, and Bingyi Kang. Bubogpt: Enabling visual grounding in multi-modal llms. *arXiv:2307.08581*, 2023. 2
- [76] Deyao Zhu, Jun Chen, Xiaoqian Shen, Xiang Li, and Mohamed Elhoseiny. MiniGPT-4: Enhancing vision-language understanding with advanced large language models. In *ICLR*, 2024. 2
- [77] Haigang Zhu, Xiaogang Chen, Weiqun Dai, Kun Fu, Qixiang Ye, and Jianbin Jiao. Orientation robust object detection in aerial images using deep convolutional neural network. In *ICIP*, 2015. 6, 7
- [78] Xiangyang Zhu, Renrui Zhang, Bowei He, Ziyu Guo, Ziyao Zeng, Zipeng Qin, Shanghang Zhang, and Peng Gao. Pointclip v2: Prompting clip and gpt for powerful 3d open-world learning. In *ICCV*, 2023. 2
- [79] Usman Zia, M Mohsin Riaz, and Abdul Ghafoor. Transforming remote sensing images to textual descriptions. *International Journal of Applied Earth Observation and Geoinformation*, 2022. 3



# SATGround : A Spatially-Aware Approach for Visual Grounding in Remote Sensing

## Supplementary Material

### 6. Analysis of grounding and referring expression detection

In Fig. 6, we provide a detailed breakdown of the quantitative visual grounding results reported in Tab. 1 of the main paper. For each respective category, we provide a cumulative distribution curve of the IoU quantiles per fraction of samples, where higher curves are better. The cumulative curves allow for more fine-grained insights into the visual grounding results. They further confirm that our method outperforms the text token-based grounding methods InternVL and Earthdial for any considered quantile on all of the respective categories. For instance, for “Large” objects, our method has  $\approx 54\%$  samples with an IoU score smaller than 0.5, compared to  $\approx 67\%$  for InternVL and Earthdial. The performance disparity is particularly visible in the “Referring: Multi” and “Grounding: Single” categories. The baseline models, InternVL and EarthDial, yield an IoU of 0 for  $\approx 40\%$  of the samples within these challenging subsets. In contrast, our method successfully establishes spatial overlap ( $\text{IoU} > 0$ ) significantly earlier in the distribution.

### 7. Inference-time sampling

We specify our visual grounding approach based on the custom control tokens  $\langle bb \rangle, \langle loc \rangle$  in Sec. 3.2 of the main paper. During inference time, we apply a greedy sampling scheme to obtain an answer sequence  $\mathbf{a} \in \mathcal{V}^{N_a}$  and bounding box coordinates  $\ell \in \mathbb{R}^{L \times 5}$  from the model for a given query sequence  $\mathbf{q} \in \mathcal{V}^{N_q}$  and reference image  $\mathbf{x} \in \mathbb{R}^{H \times W \times 3}$ . We provide a detailed description of this inference-time algorithm in Fig. 5. Whenever the model produces a  $\langle bb \rangle$  token, we do not query the LLM and instead produce a  $\langle loc \rangle$  token in a fully deterministic manner. We further register any such occurrences of  $\langle loc \rangle$  tokens and use the resulting features to query our grounding module  $\phi_{\text{grounding}}$  at the very end.

### 8. Additional qualitative results

We provide additional qualitative comparisons for grounding localization in Figs. 7 to 9, analogous to Fig. 4 in the main paper. In each instance, we depict predictions from our approach, InternVL, EarthDial, and the ground-truth bounding boxes, which are visualized in green, orange, yellow, and red, respectively.

These comparisons clearly highlight the benefits of visual grounding over conventional detection approaches, al-

---

#### Algorithm 1 Greedy sampling

---

**Input:** Image  $\mathbf{x} \in \mathbb{R}^{H \times W \times 3}$ , query  $\mathbf{q} \in \mathcal{V}^{N_q}$   
**Returns:** Answer tokens  $(\mathbf{a}_1, \dots, \mathbf{a}_{N_a}) \in \mathcal{V}^{N_a}$ , bounding box parameters  $\ell \in \mathbb{R}^{L \times 5}$

- 1: *// Compute visual  $\hat{\mathbf{x}}$  and textual  $\hat{\mathbf{q}}$  embeddings:*  
 $\hat{\mathbf{x}} \leftarrow \phi_{\text{projector}} \circ \phi_{\text{visual}}(\mathbf{x}) \in \mathbb{R}^{P \times D}$   
 $\hat{\mathbf{q}} \leftarrow \phi_{\text{embed}}(\mathbf{q}) \in \mathbb{R}^{N_q \times D}$
- 2:  $\mathbf{a}_0 \leftarrow \emptyset$
- 3: **for**  $t = 1$  to  $N_a$  **do** *// Iteratively generate tokens*
- 4:   **if**  $\mathbf{a}_{t-1} = \langle eos \rangle$  **then**
- 5:     **Break** *// Stop generation after EOS*
- 6:   **else if**  $\mathbf{a}_{t-1} = \langle bb \rangle$  **then**
- 7:     *// Deterministic  $\langle loc \rangle$  after  $\langle bb \rangle$  token:*  
 $\mathbf{a}_t \leftarrow \langle loc \rangle$
- 8:   **else**
- 9:     *// Query next token from the LM:*  
 $\hat{\mathbf{a}}_t \leftarrow \phi_{\text{lm}}(\hat{\mathbf{x}}, \hat{\mathbf{q}} | \mathbf{a}_t)$   
 $\mathbf{a}_t \leftarrow \phi_{\text{lm-head}}(\hat{\mathbf{a}}_t) \in \bar{\mathcal{V}}$
- 10:   **end if**
- 11: **end for**
- 12: *// Extract location tokens, query grounding module:*  
 $\hat{\mathbf{a}}_{\text{loc}} \leftarrow \{\hat{\mathbf{a}}_t \in \mathbb{R}^D | \mathbf{a}_t = \langle loc \rangle\} \in \mathbb{R}^{L \times D}$   
 $\ell \leftarrow \phi_{\text{grounding}}(\hat{\mathbf{a}}_{\text{loc}})$
- 13: **return**  $\mathbf{a}, \ell$

---

Figure 5. **Pseudocode for greedy sampling in our model.** The model’s LM head  $\phi_{\text{lm-head}}$  selects the most probable token at each step without randomness. After all answer tokens are generated, we additionally query the grounding module  $\phi_{\text{grounding}}$  to predict a set of bounding box parameters for each instance of a predicted location token  $\mathbf{a}_t = \langle loc \rangle$ .

lowing to query the model conveniently in a chat-based manner and enabling open vocabulary object detection. For a given image, we can provide precise context about the object such as the model number of an airplane, or disambiguate multiple objects by providing the relative location (“1 harbor at the right” vs. “2 large harbors, at the top left of the image”).

This qualitative analysis further confirms that, on average, our method significantly improves the accuracy of the obtained bounding boxes compared to those of the text token-based grounding approaches.

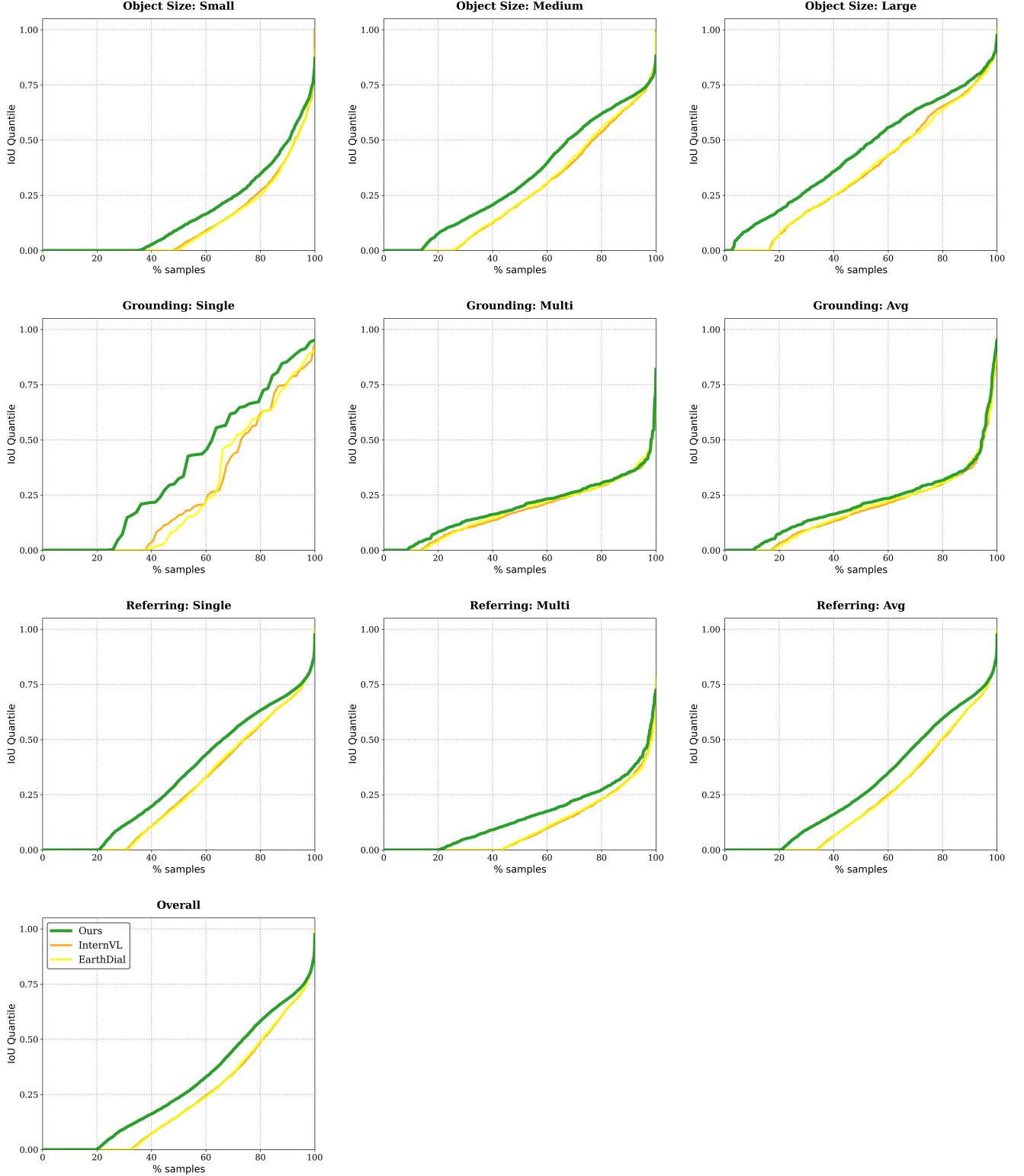


Figure 6. **Cumulative visual grounding IoU curves.** We provide a detailed analysis of the results reported in Tab. 1. For each entry in the table, we show the cumulative curve of the IoU quantile per fraction of samples; higher curves are better.

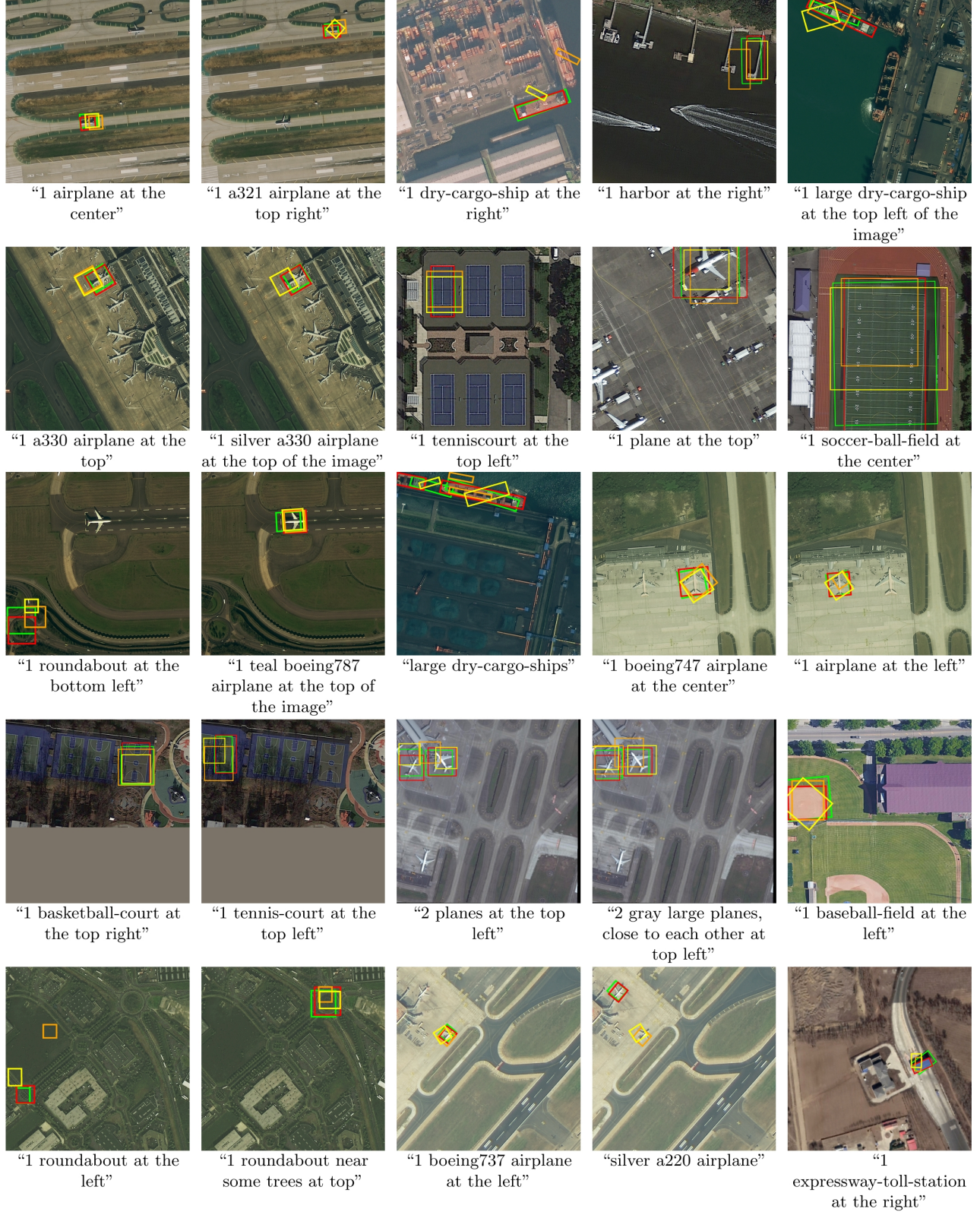


Figure 7. Visualization of additional qualitative visual grounding instances (1/3), showing predictions from our approach (green), InternVL (orange), and EarthDial (yellow) alongside the ground truth (red).





Figure 8. Visualization of additional qualitative visual grounding instances (2/3), showing predictions from our approach (green), InternVL (orange), and EarthDial (yellow) alongside the ground truth (red).



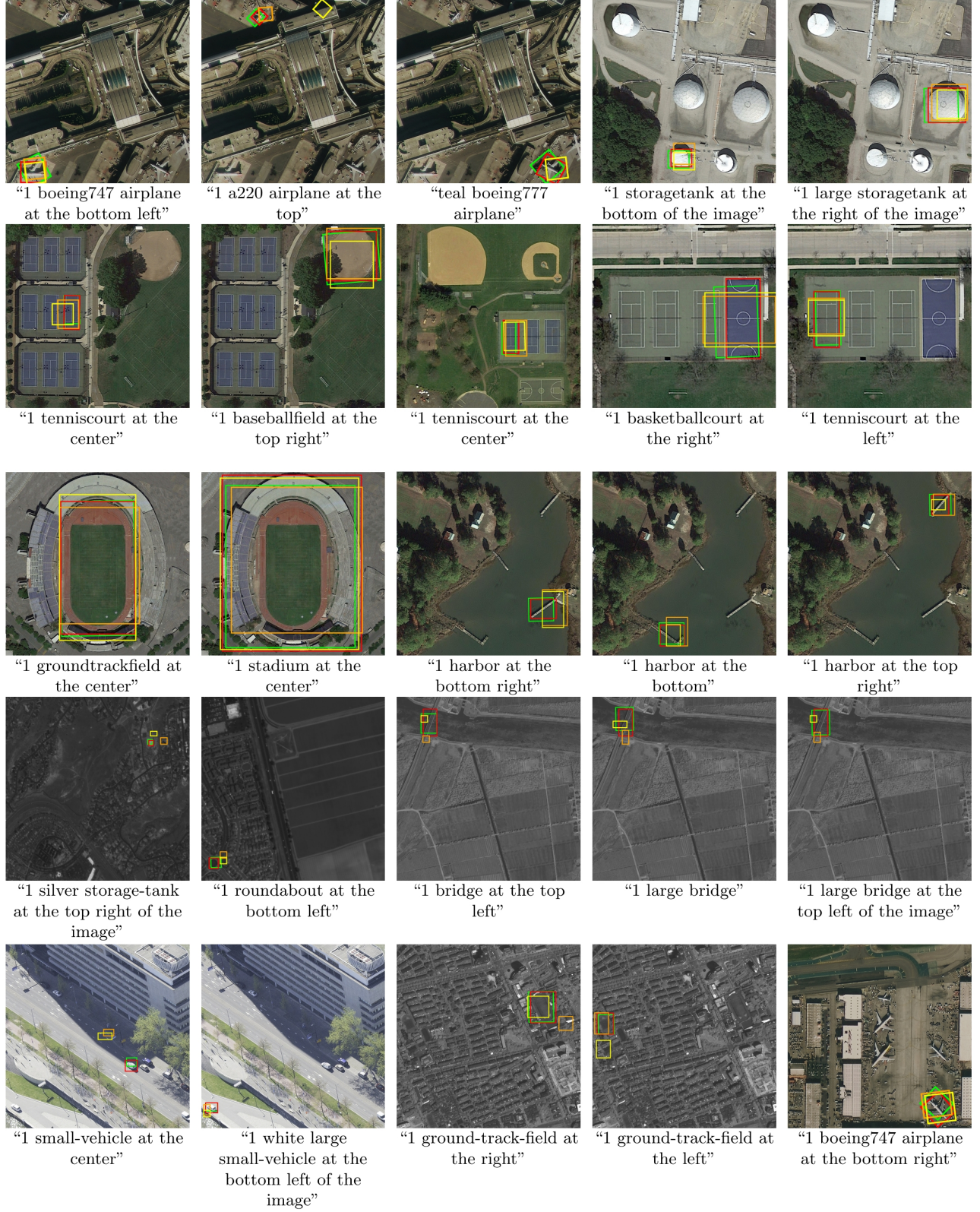


Figure 9. Visualization of additional qualitative visual grounding instances (3/3), showing predictions from our approach (green), InternVL (orange), and EarthDial (yellow) alongside the ground truth (red).